nature structural & molecular biology

Disorder-order folding transitions underlie catalysis in the helicase motor of SecA

Dimitra Keramisanou[1,4], Nikolaos Biris[1,4], Ioannis Gelis[1], Georgios Sianidis[2], Spyridoula Karamanou[2], Anastassios Economou[2,3] & Charalampos G Kalodimos[1]

SecA is a helicase-like motor that couples ATP hydrolysis with the translocation of extracytoplasmic protein substrates. As in most helicases, this process is thought to occur through nucleotide-regulated rigid-body movement of the motor domains. NMR, thermodynamic and biochemical data show that SecA uses a novel mechanism wherein conserved regions lining the nucleotide cleft undergo cycles of disorder-order transitions while switching among functional catalytic states. The transitions are regulated by interdomain interactions mediated by crucial 'arginine finger' residues located on helicase motifs. Furthermore, we show that the nucleotide cleft allosterically communicates with the preprotein substrate–binding domain and the regulatory, membrane-inserting C domain, thereby allowing for the coupling of the ATPase cycle to the translocation activity. The intrinsic plasticity and functional disorder-order folding transitions coupled to ligand binding seem to provide a precise control of the catalytic activation process and simple regulation of allosteric mechanisms.

SecA is a highly conserved and essential motor protein of the bacterial Sec translocase machinery[1]. SecA recognizes secretory proteins and couples their transport through the transmembrane SecYEG channel with the expenditure of metabolic energy provided by ATP binding and hydrolysis[2–4]. The structural relation of SecA[5–7] to superfamily-2 (SF2) DExH/D nucleic acid helicases[8,9] has raised the intriguing possibility that these proteins might use similar mechanisms to achieve translocation[7]. The helicase motor in SecA is assembled by two structurally homologous RecA-like[10] domains: the discontinuous nucleotide-binding domain (NBD; **Fig. 1a**) and the intramolecular regulator of ATP hydrolysis-2 domain (IRA2; **Fig. 1a**). The nucleotide cleft forms at the interface of NBD and IRA2 and is lined by conserved helicase motifs[1,8] (motifs I–III in NBD and motifs V and VI in IRA2), which have been suggested to link ATP binding and hydrolysis to the translocation process[11–13].

The specificity of SecA for preproteins is conferred by an attached auxiliary domain, the preprotein-binding domain[14,15] (PBD; **Fig. 1a**), which 'sprouts' out of the body of NBD through an antiparallel β-sheet. During protein translocation, a second 'specialization domain,' termed the C domain (residues 611–901 in *Escherichia coli* SecA) inserts into the membrane[16] and regulates the ATPase activity of SecA through the coordinated interaction of a 48-residue-long α-helix (scaffold domain, SD; **Fig. 1a**) with the helicase motor[17,18]. The ATPase activity of SecA is strikingly stimulated upon binding to the membrane-embedded SecYEG channel and preprotein substrates[19]. C domain–truncated SecA (residues 1–610 in *E. coli* SecA; hereafter SecAΔC) is a faithful mimic of the activated state of SecA engaged in translocation and displays similarly high stimulated enzymatic activities[17,20] and strong preprotein binding[15].

A major unresolved question regarding SecA and helicase proteins is how they convert the energy extracted from ATP binding and hydrolysis to the locomotion required for protein secretion and RNA/DNA unwinding, respectively. All NTPase motor proteins (including G proteins) sense the presence of a γ-phosphate. NTP hydrolysis and the subsequent loss of the γ-phosphate is thought to cause rearrangement of conserved structural elements flanking the NTP-binding site[21]. This rearrangement has mainly been considered to consist of a purely rigid-body movement of the two motor domains[22]. However, with the exception of very few studies[23,24], the vast majority of available crystal structures have shown rotations of the helicase motor domains that take place upon binding and release of the nucleotide[25–29], but not between the ATP- and ADP-bound states. This is somewhat surprising, because for many of these enzymes it is known that ATP hydrolysis rather than ATP binding regulates substrate affinity. For some mechanoenzymes[30–32], including SecA[5,6,33], crystal structures have suggested that no tertiary conformational changes are elicited by nucleotide binding at all.

Here, we have combined NMR, thermodynamic and biochemical approaches to characterize the *E. coli* SecA and functional derivatives at key conformational states along the catalytic pathway (apo, ATP-bound and ADP-bound). The results show that the nucleotide cleft exists in an equilibrium of well-folded and partially unfolded conformational states. Catalytic activation requires that these regions undergo disorder-order transitions, which are allosterically

[1]Department of Chemistry, Rutgers University, Newark, New Jersey 07102, USA. [2]Institute of Molecular Biology and Biotechnology, FORTH, PO Box 1385, GR-71110, Iraklio, Crete, Greece. [3]Department of Biology, University of Crete, PO Box 1527, GR-71110, Iraklio, Crete, Greece. [4]These authors contributed equally to this work. Correspondence should be addressed to C.G.K. (babis@andromeda.rutgers.edu).

Received 29 December 2005; accepted 12 May 2006; published online 18 June 2006; doi:10.1038/nsmb1108

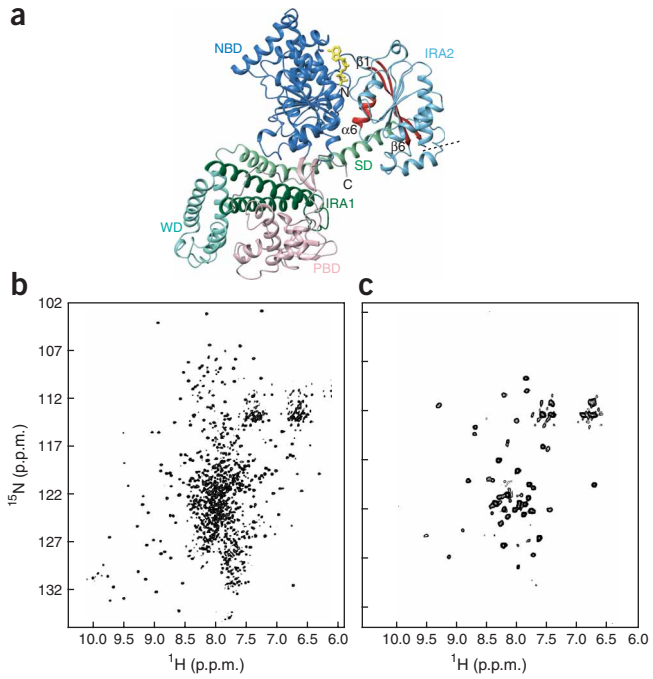

Figure 1 The helicase motor of *E. coli* SecA is intrinsically dynamic. (**a**) Crystal structure of *Bacillus subtilis* SecA bound to ADP (yellow sticks), colored according to domain organization (PDB entry 1M74)[5]. SecAΔC contains the helicase motor NBD and IRA2 domains (corresponding to domains 1a and 1b in helicases, also called nucleotide-binding folds I and II) and PBD. The C domain encompasses four substructures: SD, IRA1, WD and a C-terminal region (crystallographically unresolved)[5–7]. Regions of IRA2 identified herein to undergo disorder-order transitions are colored red. Dotted line denotes boundary of the SecAΔC fragment. (**b**) ^{1}H-^{15}N TROSY-HSQC spectrum of ^{15}N-SecAΔC (monomeric, 68 kDa) recorded at 22 °C on an 800-MHz NMR instrument. (**c**) ^{1}H-^{15}N HSQC spectrum of ^{15}N wild-type SecA (dimeric, 202 kDa) recorded at 22 °C on a 600-MHz NMR instrument. Flexibility of the helicase motor is greatly suppressed by C domain binding to SecAΔC. Only a few resonances are visible in **c**, which correspond to residues located primarily at the very flexible, crystallographically unresolved C terminus of SecA. See ref. 34 for a more detailed NMR study of the flexible regions in full-length SecA.

transmitted to PBD and are controlled by interdomain interactions among helicase motifs, by the nucleotide identity and by the action of 'arginine finger' residues. The folding transitions seem to make a particularly effective functional switch because they are reversible and inherently cooperative. The present data, combined with previous observations, suggest that this novel mechanism may be common in helicases.

RESULTS

The helicase motor of SecA is highly dynamic

To characterize the intrinsic structural and dynamic properties of the helicase motor of SecA in the ATPase-stimulated state, we characterized SecAΔC by NMR spectroscopy (**Fig. 1**). Despite its large size (68 kDa) and the fact that the protein is fully protonated, the resonance peaks of the 2D ^{1}H-^{15}N HSQC spectra appear relatively narrow (**Fig. 1b**). This indicates that SecAΔC is very dynamic. In contrast, the ^{1}H-^{15}N HSQC spectrum of intact SecA reveals extensive quench of the flexibility of the catalytic core, with only a few regions showing some mobility (**Fig. 1c**)[34]. Therefore, binding of the C domain suppresses drastically the inherent flexibility of the helicase motor. Moreover, the nucleotide-binding site in SecAΔC appears unstable, as regions of IRA2 lining the cleft (β-strands 1 and 6 and α-helix 6; red-colored regions in **Fig. 1a**) are unstructured at 22 °C, according to NOE and chemical shift index (CSI) analysis (**Supplementary Fig. 1** online). Notably, previous NMR studies have suggested that helix 6 is dynamic in solution even in full-length SecA[34], in contrast to crystallographic data showing that all these structural elements are folded[5,6,33].

The helicase motor domains interact transiently

The highly dynamic nature of SecAΔC suggests that the bi-lobar helicase motor adopts a dumbbell-like conformation in solution. A markedly 'open' conformation of the motor unit seems to be common to many helicases, as has previously been shown by crystallography for eIF4A[35], MjDEAD[36] and UAP56 DEAD-box[31,37] proteins. Nevertheless, NMR analysis shows that the cross-peaks in the isolated IRA2 domain spectra (**Fig. 2a**) are not exact subsets of SecAΔC, as considerable chemical shift perturbations are observed (**Fig. 2b**). This is suggestive of a transient, yet important interaction between IRA2 and NBD in SecAΔC (**Fig. 2c**).

IRA2 regions lining the cleft are inherently flexible

The dynamic behavior of IRA2, and its potential mechanistic implications for the regulation of the motor properties, prompted us to

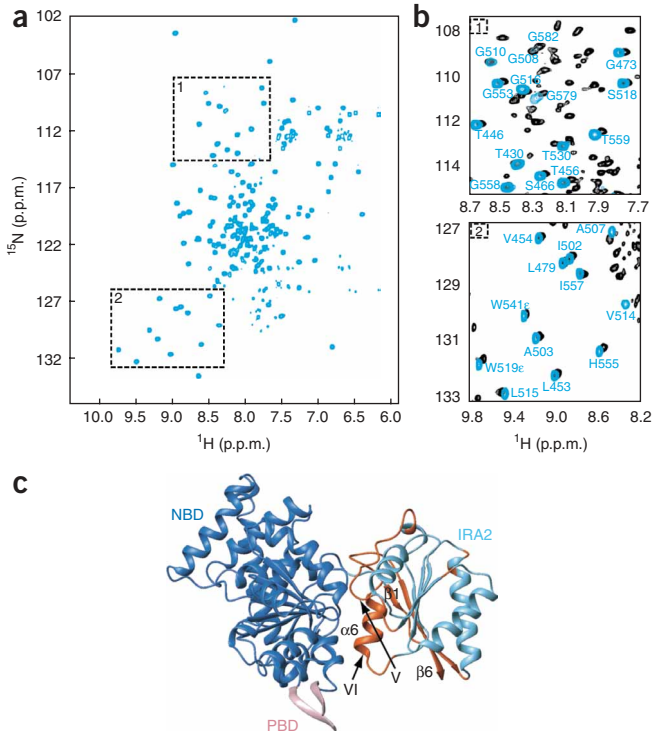

Figure 2 The helicase motor domains interact transiently. (**a**) ^{1}H-^{15}N HSQC NMR spectrum of the isolated IRA2 domain. (**b**) Excerpt of overlaid 2D ^{1}H-^{15}N HSQC spectra of isolated IRA2 (cyan) and SecAΔC (black). Assignment of the IRA2 residues is indicated. (**c**) IRA2 residues that change their chemical shift considerably upon interacting with the NBD, indicating a transient interaction between the two domains, are colored orange. Motifs V and VI, which are essential for ATP hydrolysis[7], are indicated. Results are mapped using PDB entry 1M74. β-strands 1 and 6 and α-helix 6 are unstructured in solution (**Supplementary Fig. 1**).

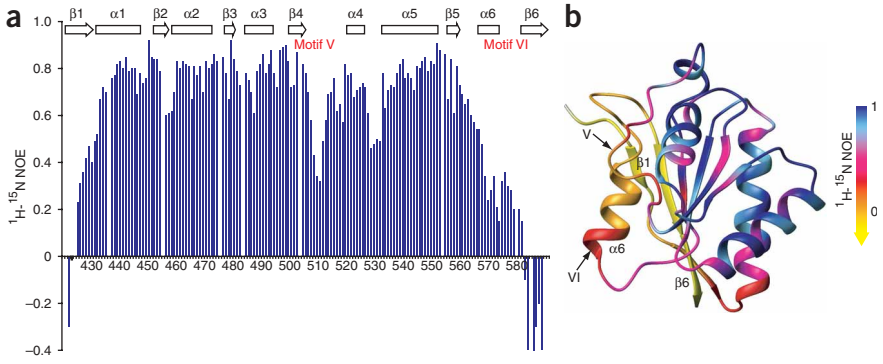

Figure 3 Fast backbone motions of isolated IRA2. (**a**) ^{1}H-^{15}N NOE values of IRA2 as a function of residue number. Low values indicate flexibility, higher values rigidity. (**b**) NOE values are mapped in continuous-scale colors on the structure of *B. subtilis* IRA2 (PDB entry 1M74). Motifs V and VI are indicated. *E. coli* IRA2 has an insertion of 29 nonconserved residues (residues 517–545) that, according to the present NOE and CSI data, form two helices, α4 and α5 (**Supplementary Fig. 1**). This insertion is remote from the NBD-IRA2 interface.

further characterize this domain. Isolated IRA2 remains structured, as evidenced by the dispersion of the NMR spectrum's resonance peaks (**Fig. 2a**) and comparison of the IRA2 NMR spectrum with that of SecAΔC (**Fig. 1b**). As in the case of SecAΔC, β-strands 1 and 6 and α-helix 6 of the isolated IRA2 are disordered (**Supplementary Fig. 1**). We next determined the amplitude of protein motions with fast (subnanosecond) time constants by recording heteronuclear ^{1}H-^{15}N NOE data (**Fig. 3a**). The measured values were mapped on the crystal structure of IRA2 (**Fig. 3b**). The motions of all residues in helicase motifs V and VI (encompassing α-helix 6) and β-strands 1 and 6 have large amplitudes (low NOE values), providing direct evidence of the pronounced flexibility of these regions. Nevertheless, the NOE values suggest that motif VI retains some residual secondary structure, as opposed to strand 6, which appears entirely unfolded (negative NOE values). In contrast, IRA2 regions that face away from the nucleotide cleft remain well folded and show substantial rigidity (**Fig. 3a**,**b**). The observed differential flexibility in IRA2 may allow the rigid part to function as a scaffold to support the dynamic region that faces the nucleotide cleft.

Nucleotide binding stabilizes a folded yet dynamic IRA2

To examine how IRA2 responds to nucleotide binding, we studied by NMR the interaction of SecAΔC with ADP. ADP binding to the motor elicits widespread conformational changes in IRA2, attested by the pronounced chemical shift changes experienced by almost all of its residues (**Fig. 4**). The resonances of several residues located close to the nucleotide interface showed particularly severe broadening, indicating the presence of conformational exchange phenomena (**Fig. 4**). Under the experimental conditions used for the NMR studies ([SecAΔC] ~0.8 mM, [ADP] ~1 mM, K_d ~0.3 μM), the contribution from ADP binding and dissociation to line broadening is negligible. This observation suggests that ADP binding to the helicase motor causes IRA2 regions surrounding the cleft to populate an ensemble of alternate conformations that interconvert on the micro- to millisecond timescale. It is noteworthy that motifs V and VI also show enhanced slow dynamics upon ADP binding (**Fig. 4b**). Such slow domain motions are biologically very important because they are close to the timescales on which functional processes such as protein folding and allosteric transitions take place[38–40]. The slow motions shown by almost all residues of IRA2 that line the nucleotide cleft suggest that these regions, which are unfolded in the absence of the nucleotide, may undergo a nucleotide-coupled disorder-order transition and populate alternate conformations in the nucleotide-bound complex. The conformational plasticity of IRA2 is potentially of great significance, because it could allow different functional states along the ATP hydrolysis pathway to be generated.

Equilibrium of disordered and ordered states in the motor

The NMR data shows that nucleotide binding induces a more ordered form of the intrinsically metastable nucleotide cleft. A very sensitive and accurate approach to characterize the disorder-order transition is to measure, by isothermal titration calorimetry (ITC)[41], changes in enthalpy (ΔH) upon nucleotide binding as a function of temperature (**Fig. 5** and **Supplementary Fig. 2** online). At low temperatures (5–20 °C), the slope of the ΔH versus temperature (T) correlation for ADP binding to SecAΔC is linear, and the heat-capacity change ($\Delta C_p = (\Delta H_1 - \Delta H_2)/(T_1 - T_2)$) is not large (**Fig. 5a**, solid blue line). This behavior is typical of protein-ligand interactions over experimental temperature ranges. Notably, at temperatures higher than 21 °C, ADP binding to SecAΔC is accompanied by an unusual nonlinear temperature dependence of the enthalpy, meaning that the heat-capacity change is temperature dependent (**Fig. 5a**, dashed blue

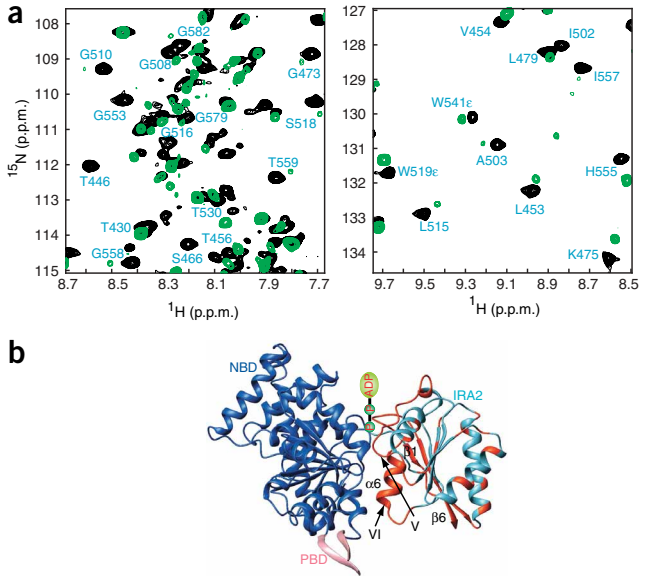

Figure 4 Effect on IRA2 induced by ADP binding to SecAΔC. (**a**) Excerpts of overlaid spectra of SecAΔC unbound (black) and bound to MgADP (green). Assignment of the IRA2 residues is indicated. (**b**) IRA2 residues whose resonance severely broadens upon ADP binding to SecAΔC are colored orange. Peak broadness signifies the presence of considerable conformational exchange, suggesting a nucleotide-induced partial folding of the intrinsically unstructured IRA2 regions that line the nucleotide cleft (β-strands 1 and 6 and α-helix 6).

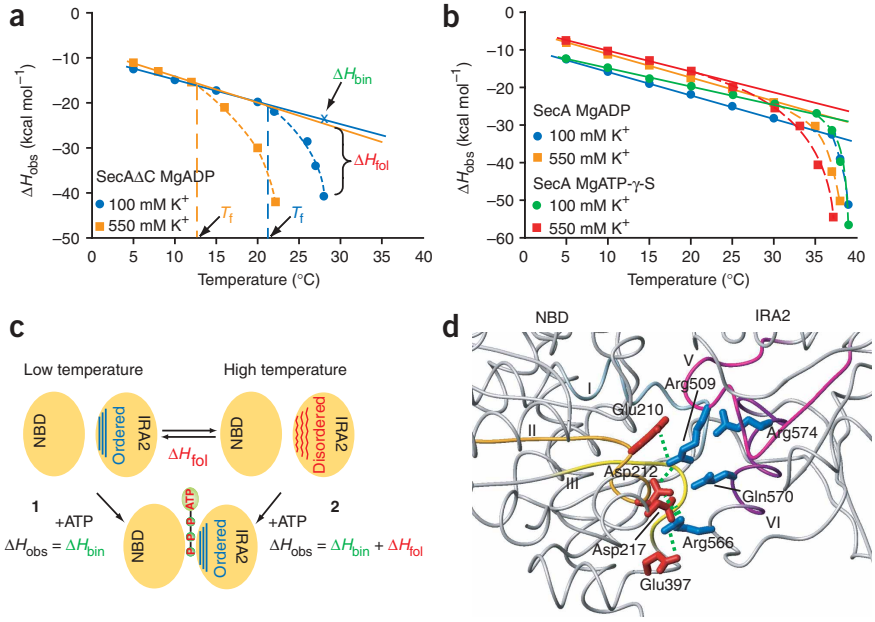

Figure 5 Thermodynamic analysis of nucleotide binding to SecAΔC and SecA. (**a**) ΔH_{obs} of MgADP binding to SecAΔC as a function of temperature in 100 mM K^+ and 550 mM K^+ buffer. Broken lines represent fits to the higher temperature points. T_f is the temperature at which the ΔH_{fol} term starts becoming appreciable, indicating disorder-order transition induced upon nucleotide binding. (**b**) ΔH_{obs} as a function of temperature for MgADP and MgATP-γ-S binding to full-length SecA in 100 mM K^+ and 550 mM K^+ buffer. (**c**) Schematic of disorder-order and binding equilibria in the nucleotide cleft at the interface of the helicase motor domains. Nucleotide binding to the cleft at low temperatures (reaction 1), where the metastable IRA2 regions lining the cleft are ordered, will give rise to observed enthalpy change (ΔH_{obs}) that corresponds in its entirety to the intrinsic nucleotide binding ΔH (ΔH_{bin}). At higher temperatures, nucleotide binding (reaction 2) induces a disorder-order transition, and an additional enthalpic term, ΔH_{fol}, appears as a result of the folding process. (**d**) Highly conserved salt bridges (green dotted lines) formed at the NBD-IRA2 interface stabilize the interaction between the domains (*E. coli* numbering). Latin numbers indicate helicase motifs. The electrostatic interactions in the nucleotide cleft give rise to the pronounced salt dependence of the thermodynamic parameters in **a** and **b**.

line). A series of similar ITC experiments conducted in buffers with different ionization enthalpies[42] showed no evidence of coupled protonation events (data not shown).

The origin of the nonlinear dependence of ΔH on temperature can be readily rationalized in terms of the observed disorder-order transition with a simple model (**Fig. 5c**). The nucleotide cleft in SecAΔC exists as an equilibrium of disordered and ordered states. At lower temperatures, the ordered states predominate, as suggested by NMR (data not shown); thus, the experimentally observed ΔH (ΔH_{obs}) upon ADP binding at temperatures below ~21 °C corresponds in its entirety to the intrinsic binding enthalpy (ΔH_{bin}) (**Fig. 5c**, reaction 1). As temperature increases, the fraction of the protein that populates the disordered states also increases (equilibrium in **Fig. 5c** shifts to the right). In this case, ADP binding would induce folding of the nucleotide cleft, in full agreement with the NMR data. As a consequence, an additional enthalpic term (ΔH_{fol}) appears (**Fig. 5c**, reaction 2). A nonzero ΔH_{fol} term is what causes ΔH_{obs} to deviate from linearity and can be used as a measure of the extent of the nucleotide-induced disorder-order transition.

Thus, the thermodynamic data strongly support the argument for the existence of a temperature-dependent equilibrium of disordered-ordered states in the nucleotide cleft of apo-SecAΔC. The increased negative heat-capacity change upon nucleotide binding at high temperatures is a characteristic of a coupled folding event[43], arising from the burial of hydrophobic surface areas as the IRA2 regions that line the cleft become more ordered. In fact, temperature-dependent heat-capacity change is the thermodynamic signature of a preexisting conformational equilibrium in the unliganded state of a protein[41,44–46]. It should be emphasized that a pure rigid-body opening and closure of the NBD-IRA2 interface cannot give rise to temperature-dependent heat capacity[44].

Interactions among helicase motifs stabilize IRA2

The characteristic temperature (referred to as T_f) at which the ΔH_{fol} term starts becoming appreciable, thus causing ΔH_{obs} to deviate from linearity, provides an additional probe of the disorder-order transition. T_f is ~21 °C for ADP binding to SecAΔC (**Fig. 5a**, blue dots). Therefore, at temperatures below T_f, the flexible regions of IRA2 lining the cleft exist in a more stable conformation in the context of SecAΔC.

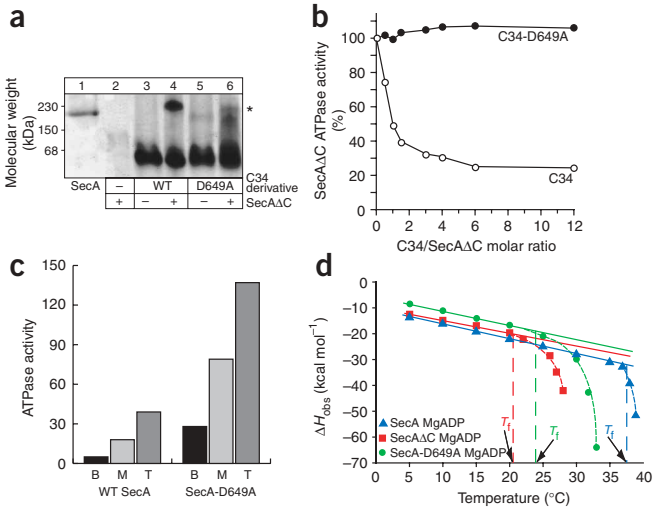

Figure 6 Effect of the D649A mutation on SecA properties. (**a**) Whereas wild-type (WT) C34 interacts with SecAΔC to yield 'reconstituted SecA' (indicated with an asterisk), C34-D649A binds SecAΔC very weakly. The reactions were analyzed by native PAGE as described previously[17]. SecAΔC does not give a sharp band in this assay (lane 2)[17]. (**b**) C34-D649A does not suppress the ATPase activity of SecAΔC, in contrast to wild-type C34. (**c**) Basal (B), membrane (M) and translocation (T) ATPase activity of wild-type SecA versus SecA-D649A. (**d**) Enthalpy change (ΔH_{obs}) as a function of temperature for the interaction of wild-type SecA, SecAΔC and SecA-D649A with MgADP in 100 mM K^+.

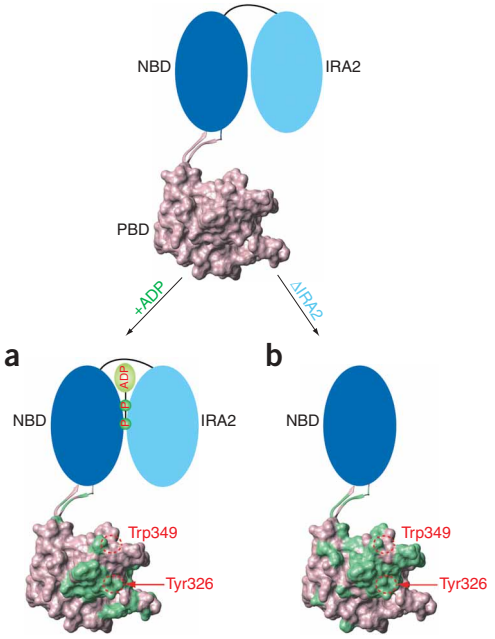

Figure 7 Allosteric effect of the presence of IRA2 and ADP binding to SecAΔC on PBD. (**a**,**b**) Schematic showing structural changes. Green surface coloring in **a** indicates residues in PBD that are affected (their resonances shift or broaden substantially) upon ADP binding; green in **b** indicates residues affected in the presence versus absence of IRA2 (**Supplementary Fig. 6**). Two residues, Tyr326 and Trp349, shown to be important for preprotein binding to SecA[15,52] are indicated. The nucleotide- and preprotein-binding sites are located more than 50 Å apart.

By contrast, NMR shows that these regions in isolated IRA2 remain unfolded and flexible even at temperatures as low as 15 °C. These IRA2 regions may gain some stability in the context of SecAΔC because of the presence of the NBD. The entire NBD-IRA2 interface is predominantly mediated by salt bridges formed by highly conserved residues at helicase motifs (**Fig. 5d**)[5,6,33].

To further test the hypothesis that the structural integrity of the nucleotide cleft depends on NBD-IRA2 interactions, the strength of the electrostatic contacts in the NBD-IRA2 interface of SecAΔC was modulated by varying the salt concentration in the buffer. Increasing the salt concentration from 100 to 550 mM K^+ caused a pronounced reduction of T_f, which approached a value of 13 °C (**Fig. 5a,** orange squares). Therefore, substantial unfolding of IRA2 takes place ~8 °C lower in the high-salt buffer than in the low-salt buffer. Owing to the 'screening' conferred by the increased concentration of salt ions, the electrostatic interactions between NBD and IRA2 are weakened; as a result, the flexible IRA2 regions facing NBD are no longer stabilized and, thus, populate unfolded states. Control of folding transitions at the nucleotide cleft by interdomain NBD-IRA2 interactions provides a mechanism to regulate the structure and dynamics of the helicase motifs as SecA undergoes conformational changes during the translocation process.

Full-length SecA undergoes disorder-order transitions

To investigate whether the disorder-order transition phenomena observed in the helicase motor of SecAΔC are influenced by the presence of the C domain, we undertook detailed thermodynamic and biochemical investigation of full-length SecA and its interaction with nucleotides. Notably, similarly to SecAΔC (**Fig. 5a**), ADP binding to SecA is also coupled to a folding transition at the nucleotide cleft (**Fig. 5b**, blue dots). However, the NBD-IRA2 interface in SecA becomes unstable only close to physiological temperatures (T_f ~37 °C), much higher than the T_f observed with SecAΔC (~21 °C). Apparently, in accordance with our NMR data (**Fig. 1b,c**) and biochemical observations[7,17,18], the presence of the C domain physically restricts the NBD and IRA2 domains from moving apart, resulting in higher stability of the regions lining the nucleotide cleft. Similarly to SecAΔC, the nucleotide-driven folding transitions in SecA are salt-dependent (**Fig. 5b**, orange squares), indicating that they rely upon electrostatic NBD-IRA2 interactions mediated by helicase motifs.

Mutations at the C domain alter the NBD-IRA2 interface

What is the structural basis for the increased stability of the NBD-IRA2 interface in SecA? The only C domain structural feature that interacts directly with both domains of the helicase motor is the SD (**Fig. 1a**)[5,6,33]. In all currently available SecA crystal structures, at least two strong salt bridges between the elongated SD α-helix and NBD appear to retain SecA in a compact conformational form. To test the hypothesis that SD regulates the integrity of the NBD-IRA2 interface, an SD-NBD salt bridge between Asp649 and Arg220 was disrupted by mutating residue Asp649 to alanine. The capacity of SecA-D649A to carry out efficient protein translocation *in vitro* and to complement a chromosomal thermosensitive *secA* gene *in vivo* is similar to that of wild-type SecA (**Supplementary Fig. 3** online). The mutation was also transferred to C34, an isolated polypeptide encompassing the complete C domain[17]. The association between C34-D649A and SecAΔC was tested using a previously established native PAGE assay[17]. In this assay, C34 binds SecAΔC, forming a 'reconstituted SecA' complex that migrates more slowly (~200 kDa; **Fig. 6a**, lane 4) than either SecAΔC (~70–100 kDa; **Fig. 6a**, lane 2) or C34 (~70 kDa; **Fig. 6a,** lane 3) alone. In contrast, C34-D649A is severely compromised in its ability to form stable complexes with SecAΔC (**Fig. 6a**, lane 6). In agreement with this result, C34-D649A does not suppress the elevated ATPase activity of SecAΔC, whereas C34 does so very efficiently (**Fig. 6b**). As expected, the basal ATPase activity of SecA-D649A compared to that of SecA is much greater (**Fig. 6c**).

To assess the effect of the D649A mutation on the integrity of the nucleotide cleft, we measured ΔH of ADP binding as a function of temperature. For ADP binding to SecA-D649A (**Fig. 6d**, green dots) the results show a much lower T_f (~24 °C), compared to wild-type SecA (T_f ~37 °C; **Fig. 6d**, blue triangles), one that approaches the characteristic T_f of SecAΔC (**Fig. 6d**, red squares). Therefore, the combined thermodynamic and biochemical data show that the SecA C domain is an additional regulator of helicase motor folding transitions and ATP catalysis.

The γ-phosphate modulates the disorder-order transition

The equilibrium of disordered-ordered states at the nucleotide cleft may be modulated during the catalytic cycle. To test this hypothesis, in addition to ADP, which probes the post-hydrolysis (or product-like) state, we used ATP-γ-S, a nonhydrolyzable ATP analog, to probe the substrate-like state. At the physiological temperature of 37 °C, ADP binding to SecA does not induce the folding transition, because the ΔH_{fol} term is 0 (**Fig. 5b**, blue dots). In contrast, at the same temperature, ATP-γ-S binding to SecA results in $\Delta H_{fol} = -4.5$ kcal mol^{-1} owing to induced folding (**Fig. 5b**, green dots). Therefore, although at 37 °C the fraction of SecA with the nucleotide cleft in the disordered state is appreciable, only ATP-γ-S binding is capable

of inducing local folding of the IRA2 regions. At higher salt concentrations, where the nucleotide cleft exists in a disordered state at low temperatures, ATP-γ-S binding induces folding of the flexible regions at a T_f of just ~25 °C (**Fig. 5b**, red squares), whereas ADP binding does so only at T_f ~32 °C (**Fig. 5b**, orange squares). These results indicate that ATP binding to SecA favors a compact conformation, rather than the relaxed one suggested previously[47] by studies using AMP-PNP, which is not a faithful mimic of ATP for SecA[48]. Overall, the thermodynamic data clearly show that the extent of the disorder-order transition is dependent on the identity of the nucleotide.

Distinct nucleotide-induced folding events are also observed in SecAΔC. The NMR results (**Figs. 1** and **2**) suggest that at 22 °C, only the IRA2 regions facing the cleft are disordered. On the basis of the amounts of nonpolar and polar surface[43] of these regions, we estimate that complete folding of IRA2 and closure of the nucleotide cleft would give rise to a ΔC_p of ~ –1 kcal mol^{-1} K^{-1}. ΔC_p due to folding (estimated by correcting for the intrinsic ΔC_p of binding at lower temperatures) is 1.4 kcal mol^{-1} K^{-1} for ATP-γ-S and 1.0 kcal mol^{-1} K^{-1} for ADP (**Supplementary Fig. 4** online). Thus, ADP binding seems to stabilize a much smaller fraction of the folded regions of IRA2 than ATP-γ-S does. Overall, ATP-γ-S and ADP modify the conformational ensemble at the NBD-IRA2 interface in distinct ways, with ATP-γ-S favoring a locally more folded state. It seems that the γ-phosphate in ATP-γ-S provides additional contacts to the flexible regions of IRA2, thus improving their stabilization.

'Arginine fingers' regulate the disorder-order transition

Arginine fingers are ubiquitous in NTPases and serve to neutralize developing charges in the transition state, thereby dramatically enhancing the catalytic activity[8,49,50]. As shown by SecA crystal structures[5,6,33], and, in accordance with structural and mutagenesis studies of relevant helicases[8], both Arg574 (motif VI) and Arg509 (motif V) in *E. coli* SecA, two highly conserved residues, could coordinate the γ-phosphate of ATP. Our results show that both R509K and R574K mutations compromise the ATPase activity of SecAΔC. Moreover, the mutants are not stimulated upon addition of preproteins and SecYEG-containing membranes to SecA (**Supplementary Fig. 5** online); such stimulation is a hallmark of the translocation process[19,51].

To determine whether these residues can function as a trigger for conformational changes during ATP hydrolysis, we measured ΔH of nucleotide binding to SecA-R574K and SecA-R509K as a function of temperature (**Supplementary Fig. 4**). ATP-γ-S binding to either SecA-R574K or SecA-R509K at 37 °C does not induce folding of the nucleotide cleft (ΔH_{fol} ~0), in contrast to wild-type SecA (ΔH_{fol} = –4.5 kcal mol^{-1}). At higher temperatures, nucleotide binding to the mutant proteins promotes some local folding, but this is to a much lesser extent than that seen in wild-type SecA. Furthermore, the dissociation constant (K_d) of the complex of either SecA-R574K or SecA-R509K with ATP-γ-S increases four-fold at 37 °C, whereas it remains invariable for their complex with ADP (**Supplementary Fig. 5**). Therefore, Arg574 and Arg509 can differentiate between ATP-γ-S and ADP and are central determinants of the alternate conformational states generated during the ATPase cycle.

Nucleotide binding affects allosterically the PBD

ADP binding to SecAΔC causes PBD to undergo dramatic changes in both its conformation (as evidenced by chemical shift changes) and slow dynamics (as evidenced by resonance broadening) (**Fig. 7a** and **Supplementary Fig. 6** online). This demonstrates that the binding signal generated at the NBD-IRA2 cleft is allosterically transmitted to PBD and affects several residues, among them Tyr326 and Trp349, that have important roles in protein translocation or respond to the presence of translocation ligands[15,52]. The substantial slow dynamics on the micro- to millisecond timescale that are induced in PBD by ADP binding to the remote helicase motor could have a great impact on the binding energetics and the promiscuous specificity[39,40] of SecA for its preprotein substrates. Notably, comparison of the NMR spectra of SecAΔC (**Fig. 1b**) with those of SecAΔC-ΔIRA2 (a polypeptide encompassing NBD and PBD, but not IRA2; **Supplementary Fig. 6**) shows that the presence of IRA2 strongly influences the conformation of PBD, even when the nucleotide cleft is vacant (**Fig. 7b**). Therefore, in addition to its role as an ATPase regulatory domain, IRA2 seems capable of affecting the preprotein-binding site at PBD. In sum, we conclude that nucleotide binding and IRA2 allosterically control both the conformation and the dynamics of the preprotein-binding site, thus providing a functional link between the ATPase cycle and preprotein binding.

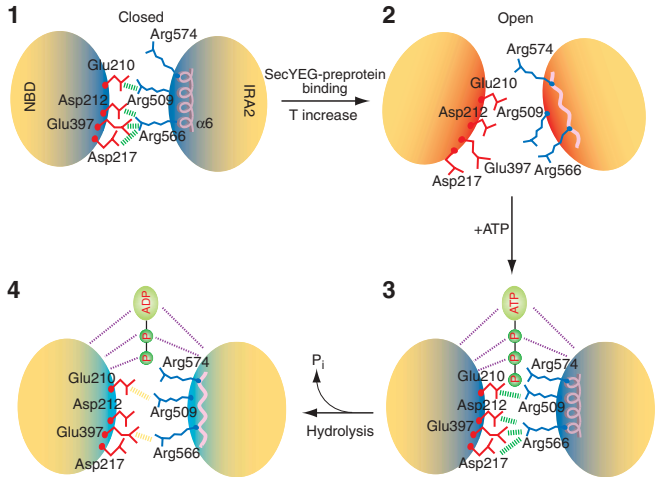

Figure 8 Model of conformational and dynamic changes in the helicase motor of SecA as a function of the nucleotide state, as suggested by the present NMR, thermodynamic and biochemical data. Green and yellow dotted lines indicate strong and weak salt electrostatic interactions, respectively. NBD-IRA2 interface is colored according to its flexibility: dark blue, light blue and red indicate increasing flexibility. PBD and C domain have been omitted for simplicity. See text for details.

DISCUSSION

The present findings demonstrate that the helicase motor of SecA has a novel allosteric mechanism that acts independently of potential rigid-body movements during the catalytic cycle. We show that, at physiological temperatures, the nucleotide cleft of SecA exists in a metastable state characterized by an equilibrium of ordered and disordered conformational states. These results are in agreement with previous observations from NMR studies of full-length SecA[34]. This highly dynamic conformational ensemble has distinct responses to ATP binding and hydrolysis, giving rise to alternate conformational states during the ATPase cycle (**Fig. 8**).

In the 'closed' conformation of the motor (**Fig. 8**, state 1), consolidated by the extensive contact surface between SD and the motor and by lower temperatures[5,47,48], NBD-IRA2 contacts are optimal and all IRA2 regions facing the cleft are well folded. Because SD is the structural 'switch' that modulates the mutual interaction of the NBD-IRA2 interface, it may then control the response of SecA to translocation ligands. Factors that loosen the SD-motor interaction

will shift the conformational equilibrium at the cleft toward the disordered state (**Fig. 8**, state 2). Notably, even a single mutation on SD that disrupts a salt bridge between SD and NBD suffices to stimulate the basal ATPase activity of SecA to values similar to those of the translocation ATPase (**Fig. 6c**). Thus, it is likely that the SD of SecA engaged in protein translocation (that is, bound to SecYEG and preproteins) undergoes cycles of detachment and rebinding to the helicase motor. The strong effect of SD in promoting the interaction between NBD and IRA2 is illustrated by the pronounced flexibility gained by SecA upon removal of the C domain (SecAΔC) (**Fig. 1b**,**c**). The flexible conformation of the motor in SecAΔC is expected to resemble the functionally relevant relaxed conformation of SecA seen at physiological temperatures[5,47,48]. However, even when SecA adopts a completely loose, dumbbell-like conformation, NBD and IRA2 still interact transiently (**Fig. 2b**,**c**) and PBD is allosterically affected (**Fig. 7b**) even in the absence of a nucleotide.

Temperature is the main determinant of the interconversion of the helicase motor between the closed and open conformations when the C domain is detached (**Fig. 8**, state 2). Whereas at elevated temperatures ADP binds SecAΔC with much lower affinity (K_d > 50 μM at 37 °C) than SecA (K_d ~1 μM at 37 °C), at low temperatures the affinities for both SecAΔC and SecA binding to ADP are very similar (K_d ~0.1 μM). Furthermore, at low temperatures the ATPase activity of SecAΔC is suppressed[17]. These measurements suggest that, whereas the helicase motor of SecAΔC is widely open at higher temperatures, drastically reducing the affinity for nucleotide, at very low temperatures it exists in a closed conformation, even in the absence of the C domain.

SecA is known to undergo an endothermic transition at temperatures slightly above physiological[5,47,48]. Because this transition is modulated by a variety of mutations in both SecA and SecG[48,53,54], as well as by the presence of nucleotides[5,7,18,53] and preproteins[15], it has been hypothesized that it is important for the preprotein translocation reaction. On the basis of combined biophysical and biochemical data, it has been proposed that this transition may involve the dissociation of the α-helical wing domain (WD; **Fig. 1a**), resulting in globally cooperative changes in domain-domain interactions and the opening of the nucleotide cleft[5,47]. The present results suggest that the disorder-order transitions at the nucleotide cleft are the primary contributor to the thermodynamics of the endothermic transition in SecA.

ATP binding to the helicase motor would bring closer the NBD and IRA2 domains by providing contacts to both of them[5,33] (**Fig. 8**, state 3). The γ-phosphate may be coordinated by Arg574 and Arg509 only when IRA2 is folded (**Supplementary Figs. 4** and **5**). Therefore, ATP binding induces a disorder-order transition resulting in the α-helix of motif VI and the other flexible regions of IRA2 becoming folded. Subsequent ATP hydrolysis and release of pyrophosphate (P_i) would disrupt the contacts of the arginine fingers to the phosphate moiety of the nucleotide, resulting in a less stable conformation (**Fig. 8**, state 4). In this state, the helicase motor is occupied by ADP and still exists in a closed conformation, as suggested by the present thermodynamic data (**Fig. 5**). This conclusion is further corroborated by earlier observations that the linker connecting NBD and IRA2 becomes protease resistant in the presence of either ATP or ADP[17]. However, it is clear from our data (**Fig. 5**) that, in contrast to the ATP-bound state, in the ADP-bound state the interdomain interactions are not optimal and regions of IRA2 facing the cleft are partially disordered.

The arginine fingers are of tantamount importance in controlling the disorder-order equilibria, as when they are mutated the resulting SecA proteins cannot differentiate between ATP and ADP. These mutants do not induce the ATP-driven disorder-order transition to the extent that wild-type SecA does (**Supplementary Fig. 4**). The overall motor conformation in the ATP-bound state of these mutant SecAs presumably resembles the ADP-bound state of wild-type SecA, as suggested by the ΔC_p values. These results reveal a previously uncharacterized role of the arginine fingers in helicase motors: their ability to modulate the degree of the conformational disorder-order transitions undergone by regions lining the nucleotide cleft. In principle, this novel mechanism may or may not be accompanied by rigid-body rotation of the motor domains, as is the mechanism described in PcrA helicase[25].

Notably, the motor domain-2 (corresponding to IRA2 in SecA) of another helicase (Hepatitis C virus, HCV)[55] seems to undergo disorder-order transitions as a function of the ligation state. A salt bridge between the helix of motif VI and the rigid scaffold of domain 2 confers stability to this region in HCV. The salt bridge is not present in IRA2 of SecA, whose stability is instead regulated through interdomain interactions with the NBD and SD. Disruption of this salt bridge in HCV by mutagenesis results in the unfolding of motif VI and two β-strands located at very similar positions to the ones seen to unfold in IRA2 (ref. 55). This observation suggests that both SecA and the HCV helicase may exploit the conformational ensemble of the helicase motor through similar mechanisms to translocate entirely different biopolymers.

In conclusion, the presence of extended regions of intrinsic plasticity at the motors of helicases provides these proteins with a very sensitive and malleable 'allosteric scaffold' that is distinctly modified during the ATPase cycle. The outcome achieved by this mechanism is the coupling of nucleotide-driven cycles of helicase motor motions to cycles of binding, conformational alteration and release of the translocated aminoacyl or nucleic acid polymer.

METHODS

Protein expression and purification. His-tagged *E. coli* SecA, SecAΔC, SecAΔC-ΔIRA2 and isolated PBD and IRA2 domains were constructed as described previously[7,15,17]. Details for the construction of R509K, R574K and D649A mutants are provided in **Supplementary Methods** (online). The BL21DE3/pLysS strain containing the selected protein-coding plasmid was grown on LB or minimal medium. Cultures for full-length SecA and its mutants were grown at 30 °C and protein synthesis was induced at the same temperature by addition of 0.5 mM of IPTG at A_{600} ~0.4. Isolated IRA2, PBD and SecAΔC-ΔIRA2 were produced by growing their cultures at 30 °C to an A_{600} ~0.3. At that point, the temperature was decreased to 22 °C and IPTG was added 1 h later. SecAΔC was produced similarly, but IPTG was added at 16 °C and the culture was allowed to grow for 2 h before harvesting. Purification for all proteins was accomplished in three steps. First, the lysate was loaded on a nickel-nitrilotriacetic acid agarose resin, pre-equilibrated with 50 mM Tris-HCl (pH 8.0), 1 M NaCl, 10% (v/v) glycerol and 5 mM imidazole. The protein was eluted with the loading buffer, containing 50–450 mM imidazole. Next, the sample was loaded, after dialysis, on a Mono-Q ion-exchange column (Amersham) and the protein was eluted with a 0–2 M NaCl linear gradient. For the final step, the sample was concentrated and applied to a Superdex-200 size-exclusion column (Amersham). Gel filtration confirmed the dimeric state of full-length SecA and the monomeric state of SecAΔC. The latter behaved as a monomer even at concentrations as high as 0.8 mM. For NMR studies, proteins were prepared as ^{15}N-, ^{13}C,^{15}N- or ^{2}H,^{13}C,^{15}N-labeled samples using minimal media containing a combination of $^{15}NH_4Cl$, $^{1}H_7$, $^{13}C_6$-glucose or $^{2}H_7$,$^{13}C_6$-glucose.

NMR spectroscopy. NMR experiments were performed on Varian 600- and 800-MHz spectrometers. Sequential assignment of the ^{1}H, ^{13}C and ^{15}N protein backbone chemical shifts was achieved by means of through-bond heteronuclear scalar correlations using the following 3D pulse sequences: 3D HNCO, 3D HN(CA)CO, 3D HNCA, 3D HN(CO)CA, 3D HNCACB and 3D HN(CO)CACB. Side chain assignment was performed using 3D C(CO)NH and

3D H(CCO)NH spectra. NOEs were assigned and collected on the basis of 3D ^{15}N NOESY HSQC and ^{13}C NOESY HSQC spectra. All NMR samples were prepared in 50 mM KCl, 50 mM potassium phosphate, 1 mM DDT and 1 g l^{-1} NaN_3 (pH 7.5). Concentrations were 0.5 mM for full-length SecA, 0.8 mM for SecAΔC, 0.5 mM for IRA2, 0.7 mM for PBD and 0.15 mM for SecAΔC-ΔIRA2. All spectra were recorded at 22 °C.

Spin relaxation measurements. The heteronuclear cross-relaxation ^{1}H-^{15}N NOE data were obtained by recording interleaving pulse sequences with and without proton saturation. One spectrum was recorded with a 3-s recycle delay followed by 3-s saturation and another spectrum with no saturation and a 6-s recycle delay. The heteronuclear ^{1}H-^{15}N NOE was determined from the ratio of peak heights for experiments with and without ^{1}H-saturation pulses.

Isothermal titration calorimetry. ITC was used to measure the enthalpy (ΔH), entropy (ΔS) and free energy (ΔG) changes of nucleotide binding to SecA and its functional derivatives. The heat capacity (ΔC_p) of the reaction was determined from the temperature dependence of enthalpy change. At least two independent measurements of the reaction were made at lower temperatures and four or five for the reactions at higher temperatures. All experiments were performed on a VP-ITC microcalorimeter (MicroCal). Protein samples were extensively dialyzed against ITC buffer, typically containing 50 mM Tris-HCl (pH 7.5), 50 mM KCl (or 500 mM KCl for experiments in high salt), 5 mM $MgCl_2$ and 1 mM TCEP. The heat of binding in the Tris buffer was very similar to that observed in potassium phosphate, indicating a weak coupling of binding to changes in protonation[42] of the protein, the ligand or both. Nucleotide solutions were prepared in the flow-through of the last buffer exchange and their concentration was determined spectrophotometrically using a molecular extinction coefficient of 14,650 M^{-1} cm^{-1} at 259 nm. More experimental details are provided in **Supplementary Figure 2**.

Note: Supplementary information is available on the Nature Structural & Molecular Biology website.

ACKNOWLEDGMENTS

We wish to thank L. Gierasch for helpful discussions, F. Jordan for the use of the VP-ITC, Y. Papanikolau and K. Petratos for sharing data before publication, S. Papanikou and B. Pozidis for help with chromatography and R. Monteiro, A. Khan and M. Vougioukalaki for experiments performed during their undergraduate training. Initial experiments were supported by an EU large-scale facility grant to SON-NMR Utrecht, The Netherlands. Research was supported by a Scientist Development Grant from the American Heart Association (to C.G.K.), a Johnson & Johnson Discovery Award (to C.G.K.), a Rutgers Busch grant (to C.G.K.), grants from the EU (RTN1-1999-00149, QLK3-CT-2000-00082 and QLK3-CT-2000-00082; to A.E), Pfizer, Inc. and grants from the Greek General Secretariat of Research (01AKMON46 and PENED03ED623; to A.E).

COMPETING INTERESTS STATEMENT

The authors declare that they have no competing financial interests.

Published online at http://www.nature.com/nsmb/
Reprints and permissions information is available online at http://npg.nature.com/reprintsandpermissions/

1. Vrontou, E. & Economou, A. Structure and function of SecA, the preprotein translocase nanomotor. *Biochim. Biophys. Acta* **1694**, 67–80 (2004).
2. Driessen, A.J., Manting, E.H. & van der Does, C. The structural basis of protein targeting and translocation in bacteria. *Nat. Struct. Biol.* **8**, 492–498 (2001).
3. Mori, H. & Ito, K. The Sec protein-translocation pathway. *Trends Microbiol.* **9**, 494–500 (2001).
4. Osborne, A.R., Rapoport, T.A. & van den Berg, B. Protein translocation by the Sec61/Secy channel. *Annu. Rev. Cell Dev. Biol.* **21**, 529–550 (2005).
5. Hunt, J.F. *et al.* Nucleotide control of interdomain interactions in the conformational reaction cycle of SecA. *Science* **297**, 2018–2026 (2002).
6. Sharma, V. *et al.* Crystal structure of *Mycobacterium tuberculosis* SecA, a preprotein translocating ATPase. *Proc. Natl. Acad. Sci. USA* **100**, 2243–2248 (2003).
7. Sianidis, G. *et al.* Cross-talk between catalytic and regulatory elements in a DEAD motor domain is essential for SecA function. *EMBO J.* **20**, 961–970 (2001).
8. Caruthers, J.M. & McKay, D.B. Helicase structure and mechanism. *Curr. Opin. Struct. Biol.* **12**, 123–133 (2002).
9. Tanner, N.K. & Linder, P. DExD/H box RNA helicases: from generic motors to specific dissociation functions. *Mol. Cell* **8**, 251–262 (2001).
10. Story, R.M., Weber, I.T. & Steitz, T.A. The structure of the *E. coli* recA protein monomer and polymer. *Nature* **355**, 318–325 (1992).
11. Papanikou, E. *et al.* Helicase Motif III in SecA is essential for coupling preprotein binding to translocation ATPase. *EMBO Rep.* **5**, 807–811 (2004).
12. Delagoutte, E. & von Hippel, P.H. Helicase mechanisms and the coupling of helicases within macromolecular machines. Part I: structures and properties of isolated helicases. *Q. Rev. Biophys.* **35**, 431–478 (2002).
13. Rocak, S. & Linder, P. DEAD-box proteins: the driving forces behind RNA metabolism. *Nat. Rev. Mol. Cell Biol.* **5**, 232–241 (2004).
14. Baud, C. *et al.* Allosteric communication between signal peptides and the SecA protein DEAD motor ATPase domain. *J. Biol. Chem.* **277**, 13724–13731 (2002).
15. Papanikou, E. *et al.* Identification of the preprotein binding domain of SecA. *J. Biol. Chem.* **280**, 43209–43217 (2005).
16. Economou, A. & Wickner, W. SecA promotes preprotein translocation by undergoing ATP-driven cycles of membrane insertion and deinsertion. *Cell* **78**, 835–843 (1994).
17. Karamanou, S. *et al.* A molecular switch in SecA protein couples ATP hydrolysis to protein translocation. *Mol. Microbiol.* **34**, 1133–1145 (1999).
18. Vrontou, E., Karamanou, S., Baud, C., Sianidis, G. & Economou, A. Global coordination of protein translocation by the SecA IRA1 switch. *J. Biol. Chem.* **279**, 22490–22497 (2004).
19. Lill, R., Dowhan, W. & Wickner, W. The ATPase activity of SecA is regulated by acidic phospholipids, SecY, and the leader and mature domains of precursor proteins. *Cell* **60**, 271–280 (1990).
20. Triplett, T.L. *et al.* Functional signal peptides bind a soluble N-terminal fragment of SecA and inhibit its ATPase activity. *J. Biol. Chem.* **276**, 19648–19655 (2001).
21. Schliwa, M. & Woehlke, G. Molecular motors. *Nature* **422**, 759–765 (2003).
22. Ye, J., Osborne, A.R., Groll, M. & Rapoport, T.A. RecA-like motor ATPases–lessons from structures. *Biochim. Biophys. Acta* **1659**, 1–18 (2004).
23. Gai, D., Zhao, R., Li, D., Finkielstein, C.V. & Chen, X.S. Mechanisms of conformational change for a replicative hexameric helicase of SV40 large tumor antigen. *Cell* **119**, 47–60 (2004).
24. Mancini, E.J. *et al.* Atomic snapshots of an RNA packaging motor reveal conformational changes linking ATP hydrolysis to RNA translocation. *Cell* **118**, 743–755 (2004).
25. Velankar, S.S., Soultanas, P., Dillingham, M.S., Subramanya, H.S. & Wigley, D.B. Crystal structures of complexes of PcrA DNA helicase with a DNA substrate indicate an inchworm mechanism. *Cell* **97**, 75–84 (1999).
26. Korolev, S., Hsieh, J., Gauss, G.H., Lohman, T.M. & Waksman, G. Major domain swiveling revealed by the crystal structures of complexes of *E. coli* Rep helicase bound to single-stranded DNA and ADP. *Cell* **90**, 635–647 (1997).
27. Karpowich, N. *et al.* Crystal structures of the MJ1267 ATP binding cassette reveal an induced-fit effect at the ATPase active site of an ABC transporter. *Structure* **9**, 571–586 (2001).
28. Wang, J. Nucleotide-dependent domain motions within rings of the RecA/AAA(+) superfamily. *J. Struct. Biol.* **148**, 259–267 (2004).
29. Savvides, S.N. *et al.* VirB11 ATPases are dynamic hexameric assemblies: new insights into bacterial type IV secretion. *EMBO J.* **22**, 1969–1980 (2003).
30. Bernstein, D.A., Zittel, M.C. & Keck, J.L. High-resolution structure of the *E. coli* RecQ helicase catalytic core. *EMBO J.* **22**, 4910–4921 (2003).
31. Shi, H., Cordin, O., Minder, C.M., Linder, P. & Xu, R.M. Crystal structure of the human ATP-dependent splicing and export factor UAP56. *Proc. Natl. Acad. Sci. USA* **101**, 17628–17633 (2004).
32. Xing, X. & Bell, C.E. Crystal structures of *Escherichia coli* RecA in complex with MgADP and MnAMP-PNP. *Biochemistry* **43**, 16142–16152 (2004).
33. Osborne, A.R., Clemons, W.M., Jr. & Rapoport, T.A. A large conformational change of the translocation ATPase SecA. *Proc. Natl. Acad. Sci. USA* **101**, 10937–10942 (2004).
34. Chou, Y.T., Swain, J.F. & Gierasch, L.M. Functionally significant mobile regions of *Escherichia coli* SecA ATPase identified by NMR. *J. Biol. Chem.* **277**, 50985–50990 (2002).
35. Caruthers, J.M., Johnson, E.R. & McKay, D.B. Crystal structure of yeast initiation factor 4A, a DEAD-box RNA helicase. *Proc. Natl. Acad. Sci. USA* **97**, 13080–13085 (2000).
36. Story, R.M., Li, H. & Abelson, J.N. Crystal structure of a DEAD box protein from the hyperthermophile *Methanococcus jannaschii*. *Proc. Natl. Acad. Sci. USA* **98**, 1465–1470 (2001).
37. Zhao, R., Shen, J., Green, M.R., MacMorris, M. & Blumenthal, T. Crystal structure of UAP56, a DExD/H-box protein involved in pre-mRNA splicing and mRNA export. *Structure* **12**, 1373–1381 (2004).
38. Volkman, B.F., Lipson, D., Wemmer, D.E. & Kern, D. Two-state allosteric behavior in a single-domain signaling protein. *Science* **291**, 2429–2433 (2001).
39. Kalodimos, C.G. *et al.* Structure and flexibility adaptation in nonspecific and specific protein-DNA complexes. *Science* **305**, 386–389 (2004).
40. Akke, M. NMR methods for characterizing microsecond to millisecond dynamics in recognition and catalysis. *Curr. Opin. Struct. Biol.* **12**, 642–647 (2002).
41. Cliff, M.J., Williams, M.A., Brooke-Smith, J., Barford, D. & Ladbury, J.E. Molecular recognition via coupled folding and binding in a TPR domain. *J. Mol. Biol.* **346**, 717–732 (2005).
42. Baker, B.M. & Murphy, K.P. Evaluation of linked protonation effects in protein binding reactions using isothermal titration calorimetry. *Biophys. J.* **71**, 2049–2055 (1996).
43. Spolar, R.S. & Record, M.T., Jr. Coupling of local folding to site-specific binding of proteins to DNA. *Science* **263**, 777–784 (1994).
44. Bruzzese, F.J. & Connelly, P.R. Allosteric properties of inosine monophosphate dehydrogenase revealed through the thermodynamics of binding of inosine 5′-monophosphate

and mycophenolic acid. Temperature dependent heat capacity of binding as a signature of ligand-coupled conformational equilibria. *Biochemistry* **36**, 10428–10438 (1997).
45. Grucza, R.A., Futterer, K., Chan, A.C. & Waksman, G. Thermodynamic study of the binding of the tandem-SH2 domain of the Syk kinase to a dually phosphorylated ITAM peptide: evidence for two conformers. *Biochemistry* **38**, 5024–5033 (1999).
46. Kumaran, S., Grucza, R.A. & Waksman, G. The tandem Src homology 2 domain of the Syk kinase: a molecular device that adapts to interphosphotyrosine distances. *Proc. Natl. Acad. Sci. USA* **100**, 14828–14833 (2003).
47. den Blaauwen, T., Fekkes, P., de Wit, J.G., Kuiper, W. & Driessen, A.J. Domain interactions of the peripheral preprotein translocase subunit SecA. *Biochemistry* **35**, 11994–12004 (1996).
48. Fak, J.J. *et al.* Nucleotide exchange from the high-affinity ATP-binding site in SecA is the rate-limiting step in the ATPase cycle of the soluble enzyme and occurs through a specialized conformational state. *Biochemistry* **43**, 7307–7327 (2004).
49. Bourne, H.R. G proteins. The arginine finger strikes again. *Nature* **389**, 673–674 (1997).
50. Crampton, D.J., Guo, S., Johnson, D.E. & Richardson, C.C. The arginine finger of bacteriophage T7 gene 4 helicase: role in energy coupling. *Proc. Natl. Acad. Sci. USA* **101**, 4373–4378 (2004).
51. Or, E., Navon, A. & Rapoport, T. Dissociation of the dimeric SecA ATPase during protein translocation across the bacterial membrane. *EMBO J.* **21**, 4470–4479 (2002).
52. Kourtz, L. & Oliver, D. Tyr-326 plays a critical role in controlling SecA-preprotein interaction. *Mol. Microbiol.* **37**, 1342–1356 (2000).
53. Schmidt, M., Ding, H., Ramamurthy, V., Mukerji, I. & Oliver, D. Nucleotide binding activity of SecA homodimer is conformationally regulated by temperature and altered by prlD and azi mutations. *J. Biol. Chem.* **275**, 15440–15448 (2000).
54. Ramamurthy, V., Dapic, V. & Oliver, D. secG and temperature modulate expression of azide-resistant and signal sequence suppressor phenotypes of *Escherichia coli* secA mutants. *J. Bacteriol.* **180**, 6419–6423 (1998).
55. Liu, D., Windsor, W.T. & Wyss, D.F. Double-stranded DNA-induced localized unfolding of HCV NS3 helicase subdomain 2. *Protein Sci.* **12**, 2757–2767 (2003).